Abstract At the Institute fuer Theoretische Nachrichtentechnik und Informationsverarbeitung at the University of Hannover investigations were carried out in cooperation with the Institute of Nuclear Engineering and Non-Destructive Testing concerning 3D analysis of internal defects using stereoradioscopy based on camera modelling. A camera calibration approach is used to determine 3D position and volume of internal defects using only two different X-ray images recorded from arbitrary directions. The volume of defects is calculated using intensity evaluation considering polychromatic radiation of microfocus X-ray tubes. The system performance was determined using test samples with different types of internal defects. Using magnifications between 1.1 and 1.4 the system achieves an accuracy of 0.5mm calculating the 3D positions of defects using samples rotated only 10° between two views and an accuracy of 0.3mm using 25° rotation. During calibration the distortion inherent in the image detector system is reduced from a maximum of 3.8mm to less than 0.1mm (0.3 pixel). The defect volumes are calculated with an overall accuracy of 10%. Additional results will be presented using the system to analyse casting defects.

1 Introduction

X-ray imaging is often used to detect and to classify different internal defects, for example casting defects in metallic samples [1]. A single image does not provide real 3D information concerning the 3D positions of detected defects. Two or more images of a sample recorded from different directions have to be used to calculate the 3D positions of detected defects (for example using stereoradioscopy or X-ray tomography). We will describe a method to determine 3D position and volume of internal defects using only two X-ray images recorded from arbitrary directions. In contrast to other stereoradioscopy systems [1, 2, 3] we do not need precise control over sample movements to determine the 3D positions of defects. A simple calibration pattern is used to calculate position and orientation of sample and X-ray source relative to the image intensifier tube. The calibration is used to reduce the distortions inherent in the image detector system and to calculate the 3D defect positions (figure 1). The volumes of internal defects are calculated using intensity

evaluation. To consider the polychromatic radiation of microfocus X-ray tubes a gauge function is used.

In the following sections our approach to stereoradioscopy will be described in detail. At first, the camera model and the calibration procedure are introduced, in the second part, the calculation of 3D defect positions and the volume estimation procedure are explained.

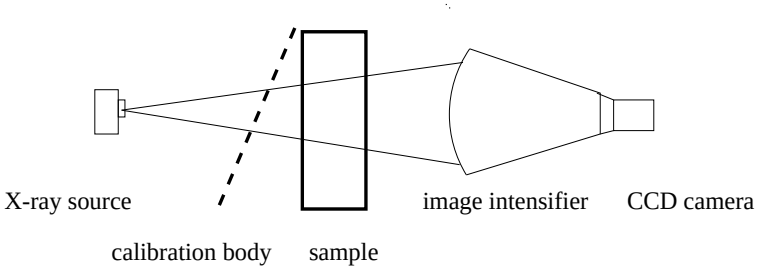

Figure 1: X-ray imaging system with calibration body and test sample

2 Geometric Calibration

To describe the X-ray imaging system the projection of 3D object points onto the 2D image plane, and nonlinear distortions inherent in the image detector system have to be modelled. A parametric camera model based on a simple pinhole model to describe the projection in combination with a polynomal model of the nonlinear distortions is used to describe the X-ray imaging system. The parameters of the model are estimated using a two step approach. First the distortion parameters for fixed source and detector positions are calculated without any knowledge of the projection parameters. In a second step, the projection parameters are calculated for each image taken with the same source and detector positions but with different sample positions.

2.1 Camera Model

In this section the camera model based on a projection model and the polynomal model of the image detector distortions will be described (figure 2).

There are two kinds of geometric distortion introduced by the image intensifier, radial distortion and S distortion. Radial distortion is due to the curvature of the input surface of the image intensifier. The mapping of electrons from the curved input surface to the flat output screen causes larger object magnification at the image periphery than at the center. In addition, the projection of objects onto the curved input surface contributes to the total radial distortion. S distortion is due to the surrounding magnetic field, for example, the earth magnetic field or nearby man-made magnetic fields. The severity of the S distortion varies with the position of the image intensifier relative to the magnetic field direction [2, 4]. The transverse component of the magnetic field causes the image to be displaced while the longitudinal field tends to rotate the image. Some minor distortions are introduced by the CCD camera.

The projection model (equations 1, 2) describes the mapping of 3D points $P_w = (x_w, y_w, z_w)^T$ to 2D image points $P_i = (x_i, y_i)^T$ in a virtual, undistorted image plane. The

3D points $P_w = (x_w, y_w, z_w)^T$ are rotated -rotation matrix **R**-, shifted -translation vector **T**- and mapped to the image plane considering scaling (S_x, S_y) of the coordinate axes and a shift (C_x, C_y) of the center of the coordinate system. The distance between X-ray source and image intensifier tube is called f.

$$P_c = (x_c, y_c, z_c)^T = \mathbf{R} * P_w + \mathbf{T} \tag{1}$$

$$P_i = (x_i, y_i)^T : \begin{cases} x_i = f/S_x * x_c/z_c + C_x \\ y_i = f/S_y * y_c/z_c + C_y \end{cases} \tag{2}$$

$$P_v = (x_v, y_v)^T : \begin{cases} x_v = f_1(x_i, y_i) \\ y_v = f_2(x_i, y_i) \end{cases} \tag{3}$$

$f_1(), f_2()$: third order (2-dimensional) polynomals

The distortion model (equations 3) describes the mapping of virtual, undistorted image points $P_i = (x_i, y_i)^T$ to distorted image points $P_v = (x_v, y_v)^T$ in the real image using third order (2-dimensional) polynomals.

The camera model has a high number of parameters with a high correlation between several parameters. Therefore, the calibration problem is a difficult nonlinear optimization problem with the well known problems of instable behaviour and local minima. In our work, an approach to separate the calibration of the distortion parameters and the calibration of the projection parameters is used to solve this problem.

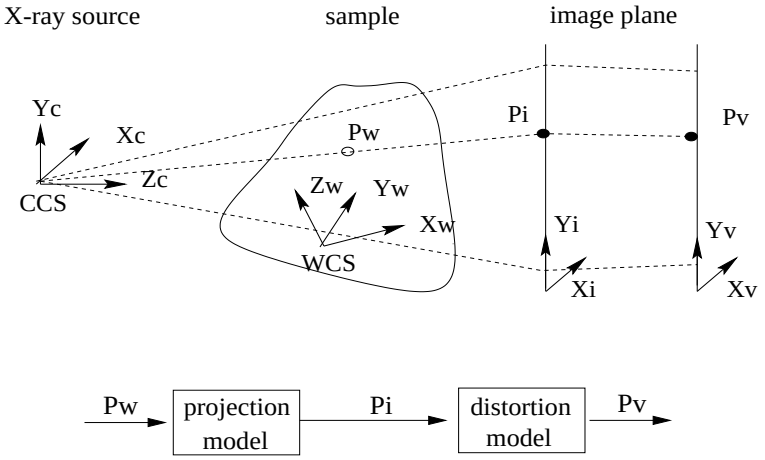

Figure 2: Camera model

2.2 Distortion Calibration

Based on the camera model the distortion parameters are calculated for fixed source and detector positions without any knowledge of the projection parameters.

A planar calibration pattern is placed in front of the image intensifier tube to calculate the distortion parameters. The calibration marks are arranged in a regular, right angled

grid with constant distances between the calibrations marks. In figure 3 a distorted image of the calibration grid is shown. Three main steps are necessary to estimate the distortion parameters. First, the distorted calibration grid is detected in the image. Second, the "nearest" regular, right angled grid is estimated, "nearest" means most similar to the distorted grid (minimum squared distances between the grid points of the measured and the regular, right angled grid). Third, the distorted grid is compared to the estimated nearest undistorted grid. The distortion parameters are estimated using a optimization procedure to minimize the squared distances between calibration marks of the estimated, "nearest" undistorted grid and the undistorted grid calculated using the distortion model. The optimization is carried out using the Levenberg-Marquart algorithm [5].

To obtain the undistorted image, for every pixel in the undistorted image the corresponding coordinates in the distorted images are calculated using the distortion model. Naturally these coordinates will about never be on the pixel grid of the distorted image. Two different interpolation methods have been implemented to calculated the desired image intensities, a high resolution cubic spline interpolation method [6] and a faster bilinear interpolation method.

The calibration of the distortion parameters depends on the position and orientation of the image intensifier relative to the surrounding magnetic field and on the position and orientation of the X-ray tube relative to the image intensifier. Therefore, the calibration has to be repeated for every change of position or orientation of the X-ray tube or the image intensifier. The calibration of the distortion parameters is independent of the position of the sample under investigation, therefore, one calibration of the distortion parameters is used for several images taken with the same fixed source and detector positions.

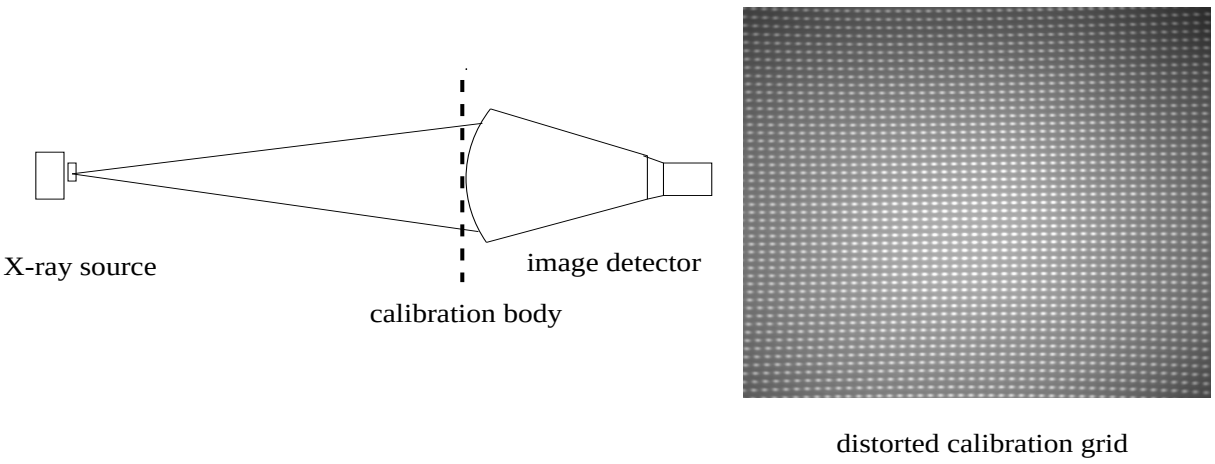

Figure 3: Distortion calibration

2.3 Calibration of the Projection Parameters

Once the distortion parameters are calibrated, undistorted images are used to estimate the projection parameters. The sample under investigation is recorded together with a calibration body. Although a 3D calibration body in general provides higher accuracy, a planar calibration body is used, because it is much easier to handle. To overcome

the problems inherent in using planar calibration bodies and to improve the accuracy of the calibration procedure, a multi image calibration strategy has been developed. To estimate the projection parameters the measured calibration marks P_i in an image are compared with the calculated projections $\tilde{P}_i$ of the 3D calibration marks onto the image plane (equation 4). As a starting point for the parameter estimation a direct estimation method is used following the approach of Tsai [7] for the calibration of CCD cameras. The nonlinear optimization is carried using the Levenberg-Marquart algorithm. The number of parameters to optimize is increased during the procedure.

$$\sum_k ||\tilde{P}_i(k) - P_i(k)||^2 \rightarrow min \tag{4}$$

Two different types of calibration marks are used in our experiments, planar circles and circular balls. The accuracy of the calibration procedure depends on the accuracy of the feature detection algorithms used to detect the calibration marks in the images. To take this in account, a special feature detection procedure based on accurate ellipses fitting has been developed. Detected calibration marks are rejected, if the feature detection procedure indicates a low reliability.

2.3.1 Multi Image Calibration

Due to the correlation of several parameters of the projection model small errors in the measured location of the calibration marks in the image may cause remarkable errors in the estimated parameters although the error in the image plane between estimated and measured locations of the landmarks is small. In such a situation the parameters are suitable to describe the mapping of 3D points located in the plane of the calibration body, but are not suitable to describe the mapping of general 3D points not located in the plane of the calibration body. To take this problem into account, two or more images of the calibration body are used concurrently to calibrate the system. The internal parameters do not change between several images taken with the same source and detector positions but different sample positions. Therefore, the internal parameters can be calibrated simultaneously for all images using an extension of the single image calibration procedure. The parameters are estimated using the squared distance of measured and projected calibration marks in all images as an optimization criterion (equation 5). The normal calibration for each image is used as a starting point for the optimization carried out using the Levenberg-Marquart algorithm. A more detailed description of this calibration procedure can be found in [8].

$$\sum_l \sum_k ||\tilde{P}_i(k,l) - P_i(k,l)||^2 \rightarrow min \tag{5}$$

3 3D Analysis

The 3D positions of internal defects are calculated with a stereoscopic approach supporting arbitrary sample manipulations using an arbitrary number of views. The volumes of the defects are calculated using intensity evaluation.

3.1 Determination of 3D Defect Positions

Two or more images of an internal defect are used to calculate the 3D position of the defect. Sample manipulations between these images can easily be interpreted as camera movements around a fixed sample. Using this interpretation of the imaging geometry, the point of intersection of rays from different source positions to the defect locations in the corresponding images determines the 3D positions of the defects. Two images are necessary to determine defect positions. If three or even more images are used, the influence of deviations of the estimated defect locations from the true locations in the images due to segmentation problems is reduced.

The epipolar constrains calculated using the estimated camera parameters restrict the search for corresponding image features in different images to a 1D search. Taking the uncertainty of the epipolar constrains into account, in our approach, the search is restricted to a small area around the epipolar lines in the images.

3.2 Calculation of Defect Volumes

The volume of defects is calculated using intensity evaluation. Considering the polychromatic radiation of microfocus X-ray tubes the X-ray beam is represented by an energy dependent intensity distribution Io(E). The intensity Ip behind a sample of thickness s is given by integrating the absorption law over all energies:

$$Ip(s) = \int Io(E)D(E) * \exp\{-(\mu(E) * s)\}dE \tag{6}$$

s: material thickness in beam direction
$Ip(s)$: image intensity
$Io(E)$: intensity in front of the sample
$D(E)$: detector sensitivity
$\mu(E)$: linear attenuation coefficient
E: radiation energy

If there is an internal defect, the image intensity is increased depending on the defect extension in beam direction.

$$Ip_F(s, d_F) = \int Io(E)D(E) * \exp\{-\mu_{Mat}(E) * s + (\mu_{Mat}(E) - \mu_{Air}(E)) * d_F\}dE \tag{7}$$

d_F: defect extension in beam direction
$Ip_F(s, d_F)$: image intensity in defect areas

To determine the volume of defects a two-dimensional gauge function G depending on the applied tube voltage U_P and the material under investigation is used to calculate material thickness in beam direction using the image intensities (equation 8). The gauge function is calculated using a calibration body.

$$s = G(U_P, Ip, \mu) \tag{8}$$

The calculated material thickness is used to estimate the volume of defects according to the following approach. Defect areas have to be detected in the images. In defect areas the intensity distribution without the influence of the defect is estimated from the surrounding intensity distribution. The defect extension in beam direction is calculated comparing the real intensity distribution in defect areas with the estimated intensity distribution without the influence of the defect (background removal). The volumes of defects are calculated integrating the defect extensions in beam direction over the defect areas considering the perspective magnification due to the perspective projection of the defects to the image plane.

4 Results

In this section results will be presented using test samples to determine the accuracy of our approach. Further on an example is shown using the system to analyse casting defects. For the experiments moderate projective magnifications between 1.1 and 1.4 were chosen. The test samples used to determine the accuracy of calibration, 3D defect position and volume estimation consist of several holes representing internal defects of different but known size and shape.

During the calibration the geometric distortions in the images are reduced from a maximum of more than 11 pixels to less than 0.3 pixels (pixel size about $0.28mm * 0.28mm$). The whole calibration results in a maximum deviation of the projected calibration marks from the measured calibration marks in the image of less than 0.4 pixel (2D-error).

Using an angle of only 10° between two views the 3D position of defects is calculated with a maximum error less than 0.5mm. Using an angle of more than 25° the maximum error is less than 0.3mm. The 3D error distribution is independent of the defect positions in the images. This indicates that the geometric distortions introduced by the image intensifier system are properly reduced. Without multi image calibration the accuracy of the calculated 3D positions decreases, the maximum error without multi image calibration is larger than 1mm. This demonstrates the advantage of the multi image calibration strategy compared to the normal calibration approach. The volume of the defects is calculated with a maximum error of about 10%. This error mainly results from problems concerning segmentation and background removal. Neglecting the influence of the polychromatic radiation, the maximum error is larger than 20%.

The system was used to analyse several casting defects of diffent size and shape using two views of each sample (rotation angle about 20° between the views). In figure 4 an original image of sample and calibration body is shown together with an enlarged image of the detected defects after background removal and defect extension estimation.

5 Conclusions

A stereoradioscopy system to calculated 3D position and volume of internal defects based on camera modelling has been presented. The results using the system to analyse test samples and to analyse several casting defects indicate the reliability of the described approach to stereoradioscopy based on camera modelling. Calibration can be used instead of a precise sample positioner for stereoradioscopic systems. The system can easily be adjusted to different sample and defect sizes using different magnifications and calibration bodies of different sizes. In the future, further work will be done using the system for tomographic reconstructions of internal defects.

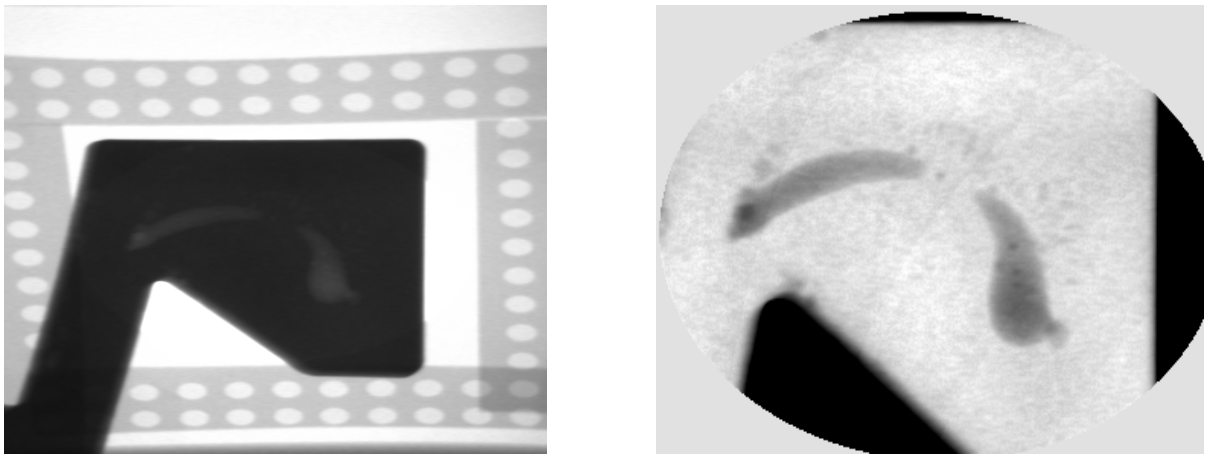

Figure 4: 3D analysis of casting defects

References

[1] Feiste, K.; Hanke, R.; Stegemann, D.; Reimche, W.: Three Dimensional Analysis of Growing Casting Defects. International Symposium on Computerized Tomography for Industrial Applications, Applications II: 20, Berlin, 1994.

[2] Doering, E.R.; Basart, J.P.; Gray, J.N.: Three-dimensional flaw reconstruction and dimensional analysis using a real-time X-ray imaging system. NDT+E International, Vol. 26(1), 1993, pp. 7–17.

[3] Hanke, R.; Böbel, F.: Determination of material flaw size by intensity evaluation of polychromatic X-ray transmission. NDT+E International, Vol. 25(2), 1992, pp. 87–93.

[4] Schueler, B.; Xiaoping H.: Correction of image intensifier distortion for three-dimensional X-ray aniography. SPIE, Vol. 2432, Physics of Medical Imaging, 1995, pp. 272–279.

[5] Press and other: Numerical recipes in C. Cambridge University Press, 1994

[6] Nijmeijer, M.C, Boer, M.A.: Correction of lens-distortion for real-time image processing systems. VLSI Signal Processing VI

[7] Tsai, R.Y.: A versatile camera calibration technique for high-accuracy 3D machine vision meterology using off-the-shell tv cameras and lenses. IEEE J.Robotics Automation, Vol. RA-3(4),August 1988, pp. 323-344.

[8] Lehr, C.: Kalibrierung von Röntgenkameras für die Lageerkennung in der Kniegelenkendoprothetik. 5. Workshop Digitale Bildverarbeitung in der Medizin, Freiburg, March 1997